arXiv:1702.02724v1 [cond-mat.str-el] 9 Feb 2017

Magnetic Frustration Driven by Itinerancy in Spinel CoV_2O_4

J. H. Lee,[1,2,*] J. Ma,[3,4,5] S. E. Hahn,[6] H. B. Cao,[7] Tao Hong,[7]
S. Okamoto,[2] H. D. Zhou,[5] M. Matsuda,[7] and R. S. Fishman[2]

[1] *School of Energy and Chemical Engineering, Ulsan National Institute of Science and Technology, Ulsan 44919, Republic of Korea*

[2] *Materials Science and Technology Division, Oak Ridge National Laboratory, Oak Ridge, Tennessee, 37831, USA*

[3] *Key Laboratory of Artificial Structures and Quantum Control, Department of Physics and Astronomy, Shanghai Jiao Tong University, Shanghai 200240, China*

[4] *Collaborative Innovation Center of Advanced Microstructures, Nanjing, Jiangsu 210093, People's Republic of China*

[5] *Department of Physics and Astronomy, University of Tennessee, Knoxville, Tennessee 37996, USA*

[6] *Neutron Data Analysis and Visualization Division, Oak Ridge National Laboratory, Oak Ridge, Tennessee 37831, USA*

[7] *Quantum Condensed Matter Division, Oak Ridge National Laboratory, Oak Ridge, Tennessee 37831, USA*

Localized spins and itinerant electrons rarely coexist in geometrically-frustrated spinel lattices. We show that the spinel CoV_2O_4 stands at the crossover from insulating to itinerant behavior and exhibits a complex interplay between localized spins and itinerant electrons. In contrast to the expected paramagnetism, localized spins supported by enhanced exchange couplings are frustrated by the effects of delocalized electrons. This frustration produces a non-collinear spin state and may be responsible for macroscopic spin-glass behavior. Competing phases can be uncovered by external perturbations such as pressure or magnetic field, which enhance the frustration.

PACS numbers: 61.05.fm, 75.10.Jm, 75.25.Dk, 75.30.Et

* jjjun97@gmail.com

The interplay between localized-spin and itinerant-electron behavior in geometrically-frustrated systems [1] is responsible for many intriguing phenomena such as a spin-liquid state [2], heavy-fermion behavior [3], spin-ice conduction [4], and exotic phases [5–7]. While the interplay between the localized spins and itinerant electrons has been investigated intensively on pyrochlores $A_2B_2O_7$ where both A and B sublattices are frustrated [2–6], it has rarely been explored on spinel systems AB_2O_4, where only the sublattice B is frustrated. In the spinels, the electronic itinerancy on sublattice B can be controlled by chemical pressure on sublattice A, which enhances magnetic frustration. On the other hand, magnetic A site ions can suppress the frustration through their magnetic interactions with the localized spins on sublattice B. Thus, one can anticipate a rich interplay between localized spins and itinerant electrons.

In the spinel vanadates AV_2O_4, the chemical pressure exerted by a small A-site cation can introduce itinerancy. Since it has the smallest magnetic A-site cation of any known spinel vanadate, CoV_2O_4 would be the ideal system to study the interplay between itinerancy and localized spins. In most spinels vanadates (AV_2O_4, A=Mn, Fe, Cd, Zn, Mg), non-collinear (NC) spin states are produced by the orbital ordering (OO) of partially-filled d-electrons on the V site, which relieves geometric frustration through a tetragonal distortion [8–14]. However, even in a cubic phase without OO, CoV_2O_4 macroscopically exhibits NC and glassy spin states [15, 16] as well as other magnetic anomalies [17]. Therefore, the NC spin states in CoV_2O_4 demand a detailed study.

Although the macroscopic spin-glass behavior of $Mn_{1-x}Co_xV_2O_4$ is enhanced by Co-doping [16], CoV_2O_4 has higher magnetic ordering temperatures than compounds $Mn_{1-x}Co_xV_2O_4$ with $x < 1$. Indeed, CoV_2O_4 has higher collinear ($T_{\rm CL}$) and NC ($T_{\rm NC}$) spin transition temperatures than any other spinel. This stands in marked contrast to the pyrochlores [5, 6], where spin-glass phases have lower ordering temperatures.

While its earlier characterization was hampered by the difficulty of fabricating single crystals, recent experiments on single crystals of CoV_2O_4 have reported anomalous physical and magnetic properties [8, 15–17]. This paper clarifies the origin of the NC spin states of CoV_2O_4 by using density functional theory (DFT) and spin models to interpret neutron-scattering measurements on CoV_2O_4 single crystals.

In contrast to previous macroscopic measurements [15, 16], our neutron scattering measurements show CoV_2O_4 to be an ordered magnet rather than a spin glass. Nevertheless, some latent factors of CoV_2O_4 can enhance frustration and drive it into a spin glass with the help of external perturbations. Chemically-driven pressure by Co increases itinerancy in CoV_2O_4. This itinerancy weakens the OO and thus enhances magnetic and structural isotropies. The frustration fostered by that isotropy [18] may be responsible for macroscopic glassy behavior in a magnetic field [15, 16]. Due to the enhanced frustration, external perturbation such as pressure or magnetic field could uncover novel magnetic phases in cubic CoV_2O_4.

Results

NC spin states in cubic phase CoV_2O_4

Figure 1 compares the temperature dependence of the (002), (220), and (111) Bragg peaks in cubic CoV_2O_4 and tetragonal MnV_2O_4. The temperature dependence of the two end-compounds was recently compared to that of the intermediates compounds $Mn_{1-x}Co_xV_2O_4$ (x = 0.2, 0.4, 0.6, 0.8) [19]. At the symmetry-allowed Bragg positions of (220) and (111), a ferrimagnetic (FIM) signals occur below T_{CL}. While the (002) peak is forbidden by structural symmetry, the observed scattering below T_{NC} indicates the formation of an antiferromagnetic (AFM) component in the ab-plane.

The (002) magnetic reflection indicates that the collinear (CL) to NC magnetic transition at T_{NC} coincides with the structural transition at T_S in MnV_2O_4 [12]. The (220) and (111) Bragg peaks show the FIM CL spin transition (T_{CL}∼150 K) and confirm recent X-ray diffraction and heat capacity measurements [16] that indicate the disappearance of the structural transition in CoV_2O_4. However, the additional magnetic transition in CoV_2O_4 indicated by the (002) peak has an enhanced transition temperature T_{NC}∼75 K compared to T_{NC}∼57 K in MnV_2O_4. Despite the induced itinerancy, this (002) peak indicates the formation of the two-in/two-out (TI/TO) spin configuration on the V-sublattice. Based on the diffraction data, this spin configuration is similar to the spin configurations in MnV_2O_4 [21] and FeV_2O_4 [22]. As shown in Supplement, the full widths at half maximum of the Bragg peaks (111) and (220) are not broadened below T_{NC}. Consequently, CoV_2O_4 is an ordered magnet and not yet a spin glass.

Although CoV_2O_4 is not a spin glass, magnetic frustration is still induced by electronic itinerancy. The ordered magnetic moment refined from the peaks in Fig. 1 is $0.47(3)\mu_B$/V in CoV_2O_4 which is significantly reduced from $0.95(4)\mu_B$/V in MnV_2O_4 due to the increased itinerancy. While the moment in CoV_2O_4 is small, the paramagnetic metallic state was expected down to zero temperature when the inter-vanadium distance R_{V-V}=2.97 Å lies below the critical value (2.98 Å) [20]. Since the TI/TO state originates from OO in tetragonal compounds [21, 22], the isosymmetric TI/TO state in cubic CoV_2O_4 without any OO must have a different origin associated with its itinerancy and frustration.

Single-ion anisotropy suppressed by itinerancy

First-principles calculations were used to explore the microscopic origin for the complex NC state in cubic CoV_2O_4. As shown in Fig. 2(a) and (c), the major magnetic anisotropy appears on the V^{3+} site with a magnitude two or three orders larger than for the *A*-site (Co/Mn). Although the V^{3+} ions are surrounded by similar octahedra in both CoV_2O_4 and MnV_2O_4 , the local [111] single-ion anisotropy (SIA) of V^{3+} is significantly reduced in CoV_2O_4 (−1.2 meV) compared to that in MnV_2O_4 (−4.8 meV) due to the melting of OO by the pressure-induced itinerancy in CoV_2O_4. Calculated by DFT, the SIA on the V sites totally disappears with an external pressure around 10 Gpa in CoV_2O_4 .

While the AFM V-V interaction in a pyrochlore lattice with local [111] SIA favors the all-in/all-out (AI/AO) spin structure, the disappearance of SIA fosters strong magnetic frustration [18]. In MnV_2O_4 , that frustration was suppressed by OO. However, the frustration reappears in CoV_2O_4 due to the melting of the OO and the suppression of the easy-axis anisotropy by itinerancy, as shown in Fig. 2(a), (b). The recovered frustration may be responsible for the macroscopic spin-glass behavior [16] below T_{NC}.

The SIA of *A*-site (Fig. 2c), (*A*=Co, Mn) is quite negligible compared to the SIA of V^{3+}. While Mn^{2+} has a weak easy-plane axis because of the compressed tetragonal structure (c/a<1), Co does not exhibit anisotropy because of the isotropic cubic structure. The SIA of Co^{2+} is much less dependent on pressure than that of V^{3+} since Co^{2+} electronic states lie significantly below the Fermi energy (ϵ_F) and are thereby electronically encapsulated, as shown in Fig. 3(a). Only V^{3+} states cross ϵ_F. Therefore the pressure-induced itinerancy will only affect the spins on V^{3+} sites.

Enhanced exchange couplings

As shown in Supplement, the Bragg peaks do not split or broaden with decreasing temperature below 100 K, indicating the absence of a strutural transition. In agreement with this measurement, DFT calculations confirm the

structural isotropy ($c/a = 1$) of CoV_2O_4 . As shown in Fig. 3, the t_{2g} (d_{xy}=d_{yz}=d_{xz}) and e_g (d_{z^2}=$d_{x^2-y^2}$) electronic levels become equally occupied and degenerate in cubic CoV_2O_4 . The structural and electronic isotropies also produce the same exchange interactions $J^{\rm in}_{\rm V-V}$=$J^{\rm out}_{\rm V-V}$=−12 meV between all spins on the tetrahedron as calculated from first principles, Fig. 4. These coupled structural, electronic, and magnetic isotropies foster frustration and the observed NC phase in Fig. 1.

Comparing the densities-of-states of CoV_2O_4 and MnV_2O_4 reveals the origin of the enhanced magnetic ordering temperatures in CoV_2O_4 . The large energy difference ($\sim$ 5 eV) between the occupied V and Mn d states weakens the exchange between Mn and V. By filling the e_g minority spin levels as indicated in Fig. 2(d) and 3(a), Co significantly lowers the t_{2g} unoccupied energy level and enhances the exchange interaction between Co and V. DFT calculations reveal that the magnitude of the AFM J_{AB} is twice as large in CoV_2O_4 (-2.5 meV) as in MnV_2O_4 (-1.2 meV). As reflected by the neutron-scattering measurements in Fig. 1, the enhanced $J_{A-\rm V}$ causes T_{CL} to more than double in CoV_2O_4 (150 K) compared to MnV_2O_4 (53K).

Strikingly, the induced itinerancy also increases the NC ordering temperature even without OO in CoV_2O_4. As shown in Fig. 1, T_{NC} significantly increases in CoV_2O_4 (75K) compared to MnV_2O_4 (57K). Although it exhibits the higher NC ordering temperature, CoV_2O_4 also exhibits glassy behavior [15, 16]. While the reduced SIA and induced isotropies foster frustration [18], the enhanced exchange interaction relieves the frustration and enhances the ordering temperatures. In the series $Mn_{1-x}Co_xV_2O_4$, the spin-wave gap ($\sim$2meV) remains relatively unchanged with Co-doping (x) [19] despite the enhanced magnetic ordering temperatures proportional to $J_{\rm A-V}$. Since the spin-wave gap is proportional to $\sqrt{D_{\rm V}\times J_{\rm A-V}}$, the increase in $|J_{\rm A-V}|$ is compensated by the reduction in the anisotropy $D_{\rm V}$ in CoV_2O_4 . By enhancing both competing effects (itinerancy-driven isotropies with reduced SIA and strengthened exchange), Co doping can foster various novel states in CoV_2O_4.

Novel phases induced by frustration

The comparison between CoV_2O_4 and MnV_2O_4 in Fig. 4 reveals the origin of the NC states in CoV_2O_4 . The key handle to tune the magnetic couplings is the distance between the V atoms ($R_{\rm V-V}$ along the x-axis) controlled by chemical doping and external pressure. In MnV_2O_4 , the OO of the V ions relieves the magnetic frustration of the pyrochlore lattice and stabilizes the TI/TO NC spin state. The AFM Mn-V interactions increase the canting angle while maintaining this TI/TO state (region **b**). By introducing itinerancy, Co doping promotes isotropic V-V interactions and favors the AI/AO spin state. Within the tetrahedron network, the AI/AO state has two distinct canting angles θ and π-θ compared to the one canting angle θ of the TI/TO state. Guided by the DFT parameters for CoV_2O_4, our model calculation indicates that the new two-angle state based on the AI/AO state lies within 0.1 meV/unit-cell of the TI/TO ground state. The isotropic exchange ($J^{\rm in}_{\rm V-V} = J^{\rm out}_{\rm V-V}$) fosters a new two-angle AI/AO structure that can be stabilized by a magnetic field.

External pressure may also increase the degree of frustration. For high external pressure [16, 17] $\sim$10 GPa, the enhanced itinerancy fully suppresses the local SIA ($D_{\rm V}$ $\sim$0) of V as in Fig. 4(a) and revives the magnetic frustration of the pyrochlore lattice. Although AFM exchange between the Co and V sites then induces the observed isosymmetric TI/TO spin structure, the frustration fostered by itinerancy and the alternative states that compete with the TI/TO ground state are responsible for the measured magnetic anomalies [17] and spin-glass behavior [16].

As shown in Figs. 2(a) and 4(a), high pressure may stabilize a continuum of degenerate states where the two angles

(θ_1, θ_2) rotate without energy cost due to the absence of SIA, as obtained in the Appendix and shown in the energy landscape of Fig. 4(d). This degeneracy can induce spin-glass or spin-liquid-like behavior. Since neutron scattering is limited to relatively low pressures, these novel states should be studied with synchrotron magnetic X-ray scattering.

Magnetic field measurement

Fig. 4(a) provides a guide to uncover the novel states produced by the regenerated frustration. Although all other magnetic couplings (isotropic $J_{\mathrm{V-V}}$, reduced D_V) foster frustration (bold red line), the remnant AFM interaction $J_{\mathrm{Co-V}}$ (dotted blue line in Fig 4(a)) still relieves frustration. An external magnetic field ($\vec{H} = H\hat{z}$) can help restore frustration by weakening $J_{\mathrm{Co-V}}$, thereby inducing the novel two-angle state of CoV_2O_4 , as shown in Fig. 5.

To check the effect of a magnetic field on CoV_2O_4, we carried out further elastic neutron-scattering measurements on the Co-rich single-crystal spinel $Co_{0.8}Mn_{0.2}V_2O_4$, which preserves the cubic structural and magnetic isotropies as in Fig. 4(a) but exhibits stronger scattering intensity than CoV_2O_4 due to the larger size of the single crystal. The V^{3+} AFM components in the *ab*-plane increase with the magnetic field ($H_z > 3$ T), as indicated by the increased intensity of (020) (see Fig. 5(a)). At $H_z < 3$ T, the increased intensity of (220) reflects the reorientation of the magnetic domains; at $H_z > 3$ T the (220) intensity is saturated, indicating that all magnetic domains are fully oriented and that the FIM components are constant. This is consistent with magnetization measurements on a polycrystalline sample, which provide a saturation field of ∼2 T [15]. Although our measurements can not disentangle the magnetic components along [001] (M_z^{Co} and M_z^{V}), we do not expect $|M_z^{\mathrm{V}}|$ to decrease with field above 3 T because that would require M_z^{Co} to further increase. So we can safely assume that both M_z^{V} and M_z^{Co} are constant above 3 T. Since the AFM components of V^{3+} in the *ab*-plane (M_{ab}^{V}) continue to grow above 3 T, the canting angle ($\theta = \tan^{-1}[M_{ab}^{\mathrm{V}}/M_z^{\mathrm{V}}]$) of the V^{3+} spins must increase with the magnetic field along [001].

Using the spin model (Eq. 1) combined with DFT parameters (Fig 4(a)), we confirm the increase in the canting angle with magnetic field in Fig. 5(c). The two-angle AI/AO state has an energy within 0.1meV/unit-cell of the the one-angle TI/TO ground state in the Co-rich region. We predict that this new state is stabilized by a large magnetic field of about 140 T, as shown in Fig. 5(c),(d). Although only the one-angle TI/TO state was previously reported in vanadate compounds (AV_2O_4, A=Zn, Mn, Fe), various competing states appear in CoV_2O_4 due to frustration. It is likely that those states can be revealed by a magnetic field or pressure.

Of course, the critical magnetic field ($H_z = 140$ T) is too large for neutron scattering measurements. However, the first-order phase transition from the one-angle to the two-angle state may be captured by magnetic susceptibility measurements. Moreover, various methods can be employed to reduce the critical field. Since external pressure suppresses SIA and revives frustration as discussed in the previous section, pressure may also reduce the critical magnetic field. Contrary to the usual expectation, a magnetic field may strengthen frustration and noncollinearity in CoV_2O_4 by weakening the only exchange coupling ($J_{\mathrm{Co-V}}$) that hampers frustration.

Discussion

It is natural to wonder if cations significantly smaller than Co^{2+} such as Be^{2+} can be substituted on the *A*-site to induce even more itinerancy and consequent frustration. However, a non-magnetic *A*-site cannot support localized V-spins so the system would become paramagnetic [20]. Because strong magnetic interactions between the *A* and *B* sites is required to maintain the localized V spins, Co is the only candidate *A*-site cation to support localized spins with enhanced $J_{\mathrm{Co-V}}$ while inducing itinerancy on the *B* site.

Compared to other vanadates (AV_2O_4), the frustration in magnetically and structurally isotropic CoV_2O_4 explains its NC and macroscopic spin-glass properties. Since the AFM interaction between Co and V is the only factor that relieves the magnetic frustration, weakening the AFM interaction by a magnetic field or further reducing the SIA by external pressure can rekindle the frustration and reveal alternative states. Among spinel vanadates, CoV_2O_4 is uniquely located at the crossover between localized and itinerant behavior. Consequently, many exotic properties and new phases can be produced by restoring the frustration of the pyrochlore lattice.

Method

Sample preparation

Single crystals of CoV_2O_4, $Co_{0.8}Mn_{0.2}V_2O_4$ and MnV_2O_4 were grown by the traveling-solvent floating-zone (TSFZ) technique. The feed and seed rods for the crystal growth were prepared by solid state reaction. Appropriate mixtures of MnO, $CoCO_3$, and V_2O_3 were ground together and pressed into 6-mm-diameter 60-mm rods under 400 atm hydrostatic pressure, and then calcined in Ar at 1050 °C for 15 hours. The crystal growth was carried out in argon in an IR-heated image furnace (NEC) equipped with two halogen lamps and double ellipsoidal mirrors with feed and seed rods rotating in opposite directs at 25 rpm during crystal growth at a rate of 20mm/h.

Neutron-scattering experiments

Single-crystal neutron diffraction was performed to determine the crystal and magnetic structures using the four-circle diffractometer (HB-3A) at the High Flux Isotope Reactor (HFIR) of the Oak Ridge National Laboratory (ORNL). A neutron wavelength of 1.003Å was used from a bent perfect Si-331 monochromator [23]. High magnetic field single-crystal neutron diffraction experiments were performed on the cold neutron triple-axis spectrometer (CTAX) at HFIR, ORNL. The incident neutron energy was selected as 5.0 meV by a PG (002) monochromator, and the final neutron energy was also set as 5.0 meV by a PG (002) analyzer. The horizontal collimation was guide-open-80′-open. Contamination from higher-order beams was removed using a cooled Be filter. The scattering plane was set in the (H,K,0) plane and the magnetic field was applied perpendicular to the scattering plane. The nuclear and magnetic structures were refined with the program FULLPROF [24]. Due to the domain re-orientation effect, intensities of both (220) and (020) diffractions increase sharply in small magnetic fields, but the (220) diffraction is saturated above about 3 T. The intensity of the (020) diffraction, corresponding to the magnetic component of V in the *ab*-plane, inceases linearly with field.

First-principles calculations

First-principles calculations were performed using density-functional theory within the local spin-density approximation with a correction due to on-site Hubbard interaction (LSDA+U) as implemented in the Vienna *ab initio* simulation package (VASP-5.3) [25]. We used the Liechtenstein [26] implementation with on-site Coulomb interaction $U = 6.0$ eV and on-site exchange interaction $J_{\rm H} = 1.0$ eV to treat the localized 3d electron states in Co, Mn, and V; this choice of U is close to that chosen in previous work on CoV_2O_4 [27] and MnV_2O_4 [28, 29]. The spin-orbit interaction was included. The projector augmented wave (PAW) potentials [30, 31] explicitly include 13 valenced electrons for Mn ($3p^6 3d^5 4s^2$), 9 for Co ($3d^8 4s^1$), 13 for V ($3s^2 3p^6 3d^4 4s^1$), and 6 for oxygen ($2s^2 2p^4$). The wave functions were expanded in a plane-wave basis with an energy cutoff of 500 eV. To evaluate the on-site single-ion anisotropy (SIA) interaction D, only one cation of interest was kept while the surrounding magnetic atoms were replaced by neutral

and isoelectronic Ca^{2+} and Al^{3+} cations for Co^{2+}/Mn^{2+} and V^{3+}, respectively. This is the same technique that was successfully used for $BiFeO_3$ [32] and $CaMn_7O_{12}$ [33].

Microscopic spin model

Spin states in spinels can be described by the following model Hamiltonian,

$$H = -\frac{1}{2}\sum_{i,j} J_{ij}\boldsymbol{S}_i \cdot \boldsymbol{S}_j + \sum_i D_i \left(\hat{u_i} \cdot \boldsymbol{S}_i\right)^2 \tag{1}$$

which contains six inequivalent sublattices. Isotropic exchange constants $J_{\mathrm{Co-V}}$ describe nearest-neighbor interactions between the Co and V sites. $J_{\mathrm{Co-Co}}$ and $J_{\mathrm{V-V}}$ describe nearest-neighbor interactions between Co-sites and V-sites, respectively. The easy-axis anisotropy is assumed to be zero for the Co-sites, while for the B-site spins, the easy-axis anisotropy D_{V} is along the local <111> direction. The azimuthal directions of each vanadium spin is constrained, but the canting angle θ_i, described in Fig. 4, is allowed to vary between 0 and 2π. Since θ_i may have a unique value in adjacent planes, both the two-in-two-out and all-in-all-out configurations are possible. These angles are equal to the polar angle when θ_i is between 0 and π, while the polar angles equals $2\pi - \theta_i$ and the azimuthal angle changes by π when θ_i is greater than π.

The ground state spin configuration was found by minimizing the classical energy for a given set of parameters. To avoid local minima, this was accomplished by calculating the classical energy on a grid with $\theta_i = 0$ to 2π and finding the two angles with the lowest energy. This process was repeated for values of the external magnetic field ranging from 0 to 173 T.

The inelastic neutron cross section for undamped spin waves was calculated using the $1/S$ formalism outlined in Ref. [34] and the qppendices of Ref. [35]. For direct comparison with experimental intensities, the effects of the magnetic form factor and the instrumental resolution were included in the calculation. The coefficients for Co^{2+}, and V^{3+} are from Ref. [36]. The resolution function was approximated as a Gaussian in energy with a full width at half-maximum of 1.5 meV. Effects from finite resolution in $\boldsymbol{Q}$ were not considered.

While DFT can provide guidance for the values of the isotropic exchange interactions, LSDA+U overestimates the experimental moment (S_{V}=0.23(7)) of CoV_2O_4 measured by neutron scattering. Our spin model uses the magnetic moment (S_{V}=0.25), which is within the experimental uncertainty. In addition, parameters calculated with DFT were adjusted to reproduce the measured canting angle of CoV_2O_4 ($\theta = 20.8 \pm 1.7^{\circ}$) in zero field. Care was also taken to avoid a long-range spiral configuration [37] that was not observed in our neutron diffraction measurements. The final set of parameters used for CoV_2O_4 are $J_{\mathrm{Co-Co}} = 0.5$meV, $J_{\mathrm{Co-V}} = -2.5$meV, $J_{\mathrm{V-V}} = -11.0$meV, $D_{\mathrm{V}} = -2.7$meV, $S_{\mathrm{Co}} = 1.50$ and $S_{\mathrm{V}} = 0.25$.

Canting angles of the new phase with D_{V}=0.0

At high pressures, we take $D_{\mathrm{V}} = 0.0$ in Eq.(1). Then, the total energy per unit magnetic unit cell is

$$E\left(\alpha\right) = -12J_{\mathrm{Co-V}}S_{\mathrm{Co}}S_{\mathrm{V}}\alpha - 4J_{\mathrm{V-V}}S_{\mathrm{V}}^2\alpha^2 + \text{constant} \tag{2}$$

where $\alpha = \cos\theta_1 + \cos\theta_2$. The total energy is at a minimum if

$$\alpha = -\frac{3J_{\mathrm{Co-V}}S_{\mathrm{Co}}}{2J_{\mathrm{V-V}}S_{\mathrm{V}}} \tag{3}$$

which limits the allowed combination of θ_1 and θ_2. When $\theta_1 = \theta_2$ and $D_{\rm Co} = D_{\rm V} = 0.0$, this condition is equal to the expression for θ in ref. [28].

Acknowledgements

The research at HFIR, ORNL, were sponsored by Department of Energy, Office of Sciences, Basic Energy Sciences, Materials Sciences and Engineering Division (J.H.L., S.O., R.F.) and Scientific User Facilities Division (J.M., S.E.H., M.M.). The research at UNIST was supported by Basic Science Research Program through the National Research Foundation of Korea (NRF) funded by the Ministry of Science, ICT & Future Planning (2.150639.01). J.M. thanks the support of the Ministry of Science and Technology of China (2016YFA0300500). S.E.H. acknowledges support by the Laboratory's Director's fund, ORNL. H.D.Z thanks the support from NSF with grant NSF-DMR-1350002. The authors acknowledge valuable discussions with G. MacDougall.

Author contributions

J.H.L. conceived the original idea and carried out first-principles calculations. S.E.H. and R.S.F. performed spin-wave simulations. J.M., H.C., T. H, and M.M. measured and analyzed neutron scattering Bragg peaks. H.D.Z. synthesized the samples. J.H.L., S.E.H., J.M., H.B.C., T.H., S.O., M.M, R.S.F. discussed the results. J.H.L. and R.F. wrote the manuscript.

Additional information

Competing finalcial interests: The authors delcare no competing financial interests.

[1] Lacroix, C., Mendels, P., & Mila, F. Introduction to Frustrated Magnetism: Materials, Experiments, Theory. *Springer*, (2001).

[2] Nakatsuji, S. *et al.* Metallic Spin-Liquid Behavior of the Geometrically Frustrated Kondo Lattice $Pr_2Ir_2O_7$. *Phys. Rev. Lett.* **96**, 087204 (2006)

[3] Lee, S.-B., Paramekanti, A., & Kim, Y.B. RKKY Interactions and the Anomalous Hall Effect in Metallic Rare-Earth Pyrochlores. *Phys. Rev. Lett.* **111**, 196601 (2013).

[4] Udagawa, M., Ishizuka, H., & Motome, Y. Non-Kondo Mechanism for Resistivity Minimum in Spin Ice Conduction Systems. *Phys. Rev. Lett.* **108**, 066406 (2012).

[5] Hanasaki, N. *et al.* Nature of the Transition between a Ferromagnetic Metal and a Spin-Glass Insulator in Pyrochlore Molybdates. *Phys. Rev. Lett.* **99**, 086401 (2007).

[6] Iguchi, S. *et al.* Emergence of a Diffusive Metal State with No Magnetic Order near the Mott Transition in Frustrated Pyrochlore-Type Molybdates. *Phys. Rev. Lett.* **102**, 136407 (2009).

[7] Kumar S. & van den Brink, J. Frustration-Induced Insulating Chiral Spin State in Itinerant Triangular-Lattice Magnets. *Phys. Rev. Lett.* **105**, 216405 (2010).

[8] Kismarahardja, A. *et al.* Dielectric properties of single crystal spinels in the series FeV_2O_4, MnV_2O_4, and CoV_2O_4 in high magnetic fields. *Phys. Rev. B* **87**, 054432 (2013).

[9] Nishiguchi, N. & Onoda, M. A pseudotetramer in the geometrically frustrated spinel system CdV_2O_4. *J. Phys. Condens. Matter* **14**, L551 (2002).

[10] Lee, S.H. *et al.* Orbital and Spin Chains in ZnV_2O_4. *Phys. Rev. Lett.* **93**, 156407 (2004).

[11] Wheeler, E. M. *et al.* Spin and orbital order in the vanadium spinel MgV_2O_4. *Phys. Rev. B* **82**, 140406(R) (2010).

[12] Garlea, V.O. *et al.* Magnetic and Orbital Ordering in the Spinel MnV_2O_4. *Phys. Rev. Lett.* **100**, 066404 (2008).

[13] MacDougall, G. J. *et al.* Magnons and a two-component spin gap in FeV_2O_4 *Phys. Rev. B* **89**, 224404 (2014).

[14] Katsufuji, T. *et al.* Structural and magnetic properties of spinel FeV2O4 with two ions having orbital degrees of freedom. *J. Phys. Soc. Jpn.* **77**, 053708 (2008).

[15] Huang, Y., Yang, Z., & Zhang, Y. Magnetic, structural, and thermal properties of CoV_2O_4. *J. Phys. Condens. Matter* **24**, 056003 (2012).

[16] Kiswandhi, A. *et al.* Chemical pressure effects on structural, magnetic, and transport properties of $Mn_{1-x}Co_xV_2O_4$, *Phys. Rev. B* **84**, 205138 (2011).

[17] Kismarahardja, A. *et al.* CoV_2O_4: A Spinel Approaching the Itinerant Electron Limit. *Phys. Rev. Lett.* **106**, 056602 (2011).

[18] Bramwell, S. T. & Harris, M. J. Frustration in Ising-type spin models on the pyrochlore lattice. *J. Phys. Condens. Matter* **10**, L215-L220 (1998).

[19] Ma, J. *el al.* Strong competition between orbital ordering and itinerancy in a frustrated spinel vanadate Phys. Rev. **B** 91, 020407 (R) (2015).

[20] Blanco-Canosa, S. *et al.* Enhanced Pressure Dependence of Magnetic Exchange in $A^{2+}[V_2]O_4$ Spinels Approaching the Itinerant Electron Limit. *Phys. Rev. Lett.* **99**, 187201 (2007).

[21] Magee, A. J. *Spin correlations in frustrated magnets with orbital ordering Ch.* 4 (Ph.D. thesis, Royal Holloway, University of London 2010).

[22] MacDougall, G. J. *et al.* Magnetic order and ice rules in the multiferroic spinel FeV_2O_4. Phys. Rev. B **86**, 060414(R) (2012).

[23] Chakoumakos, B. C. *et al.* Four-circle single-crystal neutron diffractometer at the High Flux Isotope Reactor. *J. Appl. Crystallogr.* **44**, 655 (2011).

[24] Rodrguez-Carvajal, J. Recent advances in magnetic structure determination by neutron powder diffraction. *Physica B* **192**, 55 (1993).

[25] Kresse G. & Furthmuller, J. Efficient iterative schemes for ab initio total-energy calculations using a plane-wave basis set. *Phys. Rev. B* **54**, 11169 (1996).

[26] Liechtenstein, A.I., Anisimov, V.I., & Zaanen, J. Density-functional theory and strong interactions: Orbital ordering in Mott-Hubbard insulators. *Phys. Rev. B* **52**, R5467 (1995).

[27] Kaur, R., Maitra, T., & Nautiyal., T. The nature of itineracy in CoV2O4: a first-principles study. *J. Phys.: Condens. Matter* **26**, 045505 (2014).

[28] Nanguneri, R. & Savrasov, S.Y. Exchange constants and spin waves of the orbital-ordered noncollinear spinel MnV_2O_4. *Phys. Rev. B* **86**, 085138 (2012).

[29] Sarkar, S., Maitra, T., Valentí, R., & Saha-Dasgupta, T. Proposed Orbital Ordering in MnV_2O_4 from First-Principles Calculations. *Phys. Rev. Lett.* **102**, 216405 (2009).

[30] Blochl, P. E. Projector augmented-wave method. *Phys. Rev. B* **50**, 17953 (1994).

[31] Kresse, G. & Joubert, D. From ultrasoft pseudopotentials to the projector augmented-wave method. *Phys. Rev. B* **59**, 1758 (1999).

[32] Weingart, C., Spaldin, N., & Bousquet, E. Noncollinear magnetism and single-ion anisotropy in multiferroic perovskites. *Phys. Rev. B* **86**, 094413 (2012).

[33] Zhang, J. T. *et al.* Magnetic properties and origins of ferroelectric polarization in multiferroic $CaMn_7O_{12}$. *Phys. Rev. B* **87**, 075127 (2013).

[34] Haraldsen, J. T. & Fishman, R. S. Spin rotation technique for non-collinear magnetic systems: application to the generalized

Villain model. *J. Phys.: Condens. Matter* **21**, 216001 (2009).

[35] Fishman, R. S., Haraldsen, J. T., Furukawa, N. & Miyahara, S. Spin state and spectroscopic modes of multiferroic $BiFeO_3$. *Phys. Rev. B* **87**, 134416 (2013).

[36] Dianoux, A. J. & Lander, G. *Neutron Data Booklet* (OCP Science, Philadelphia, 2003).

[37] Tomiyasu, K., Fukunaga, J., & Suzuki, H. Magnetic short-range order and reentrant-spin-glass-like behavior in $CoCr_2O_4$ and $MnCr_2O_4$ by means of neutron scattering and magnetization measurements. *Phys. Rev. B* **70**, 214434 (2004).

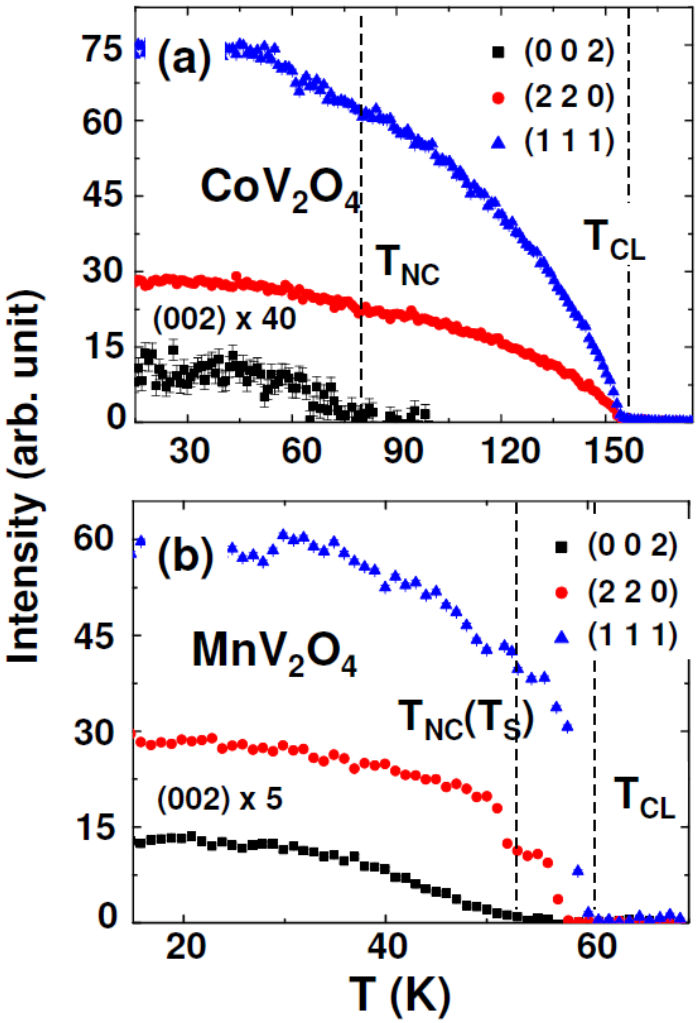

FIG. 1. **NC spin states in cubic CoV_2O_4 compared to tetragonal MnV_2O_4.** Temperature dependence of the (111) (triangles), (220) (circles), and (002) (squares) Bragg peak intensities for CoV_2O_4 **(a)** and MnV_2O_4 **(b)** measured by neutron diffraction at HB-3A. The peak intensities of (111) and (220) above the magnetic transition temperature are fully from the nuclear structure and were subtracted. The (002) peak is not allowed from the structural symmetry and fully originated from the magnetic scattering. The background was subtracted. All the magnetic peaks observed by our neutron diffraction are instrument resolution limited besides the peak broadening caused by the structural transition for MnV_2O_4, and thus indicate the long range ordered magnetic moments. The strongly-reduced intensity of (002) peak in CoV_2O_4 indicates that only tiny amount of V spin orders, which is caused by enhanced itinerancy.

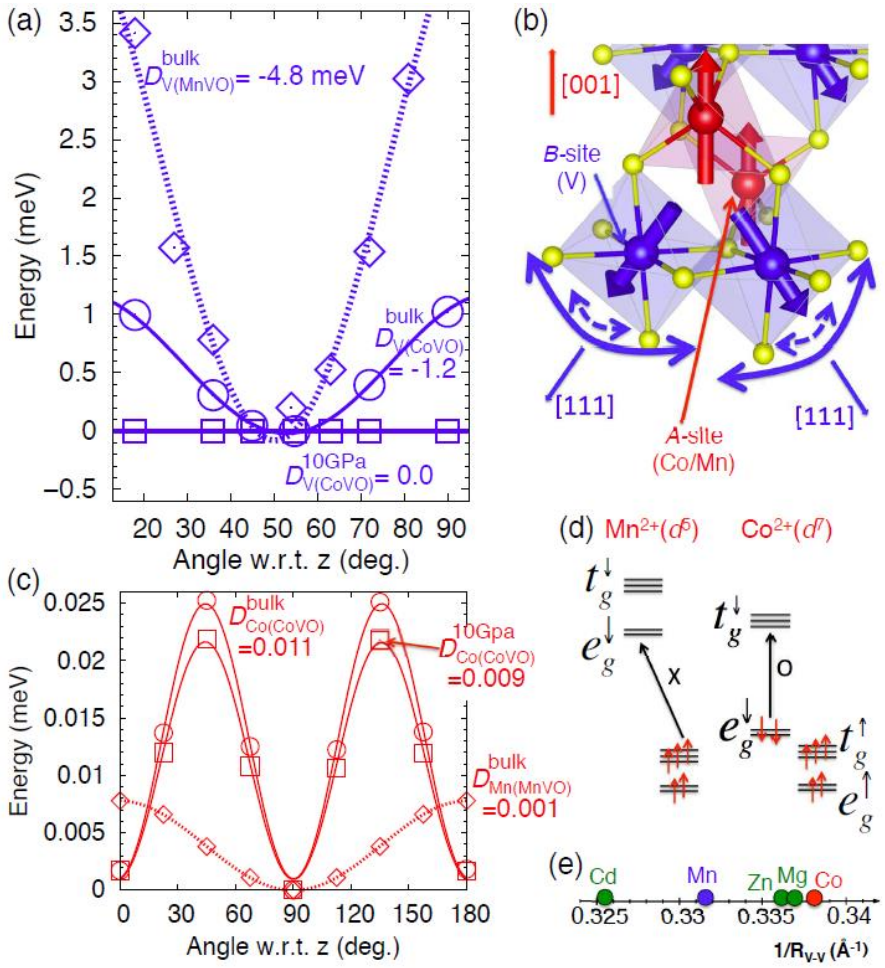

FIG. 2. **Reduced single-ion anisotropy (SIA) of V in CoV_2O_4 compared with that in MnV_2O_4.** **(a)** Total energy versus angle and associated SIA (meV) of V^{3+} in ambient (circle) and 10 GPa (square) pressure for bulk CoV_2O_4 and MnV_2O_4 (diamond). **(b)** NC spin configurations of V^{3+} and Co^{2+}/Mn^{2+} spins pointing along local [111] and global [001] directions, respectively. The round bold (dotted) arrows close to V spins depict the rotational flexibility in CoV_2O_4 (MnV_2O_4). **(c)** SIA of Co^{2+} in bulk CoV_2O_4 under 10 Gpa compared to SIA of Mn^{2+} in bulk MnV_2O_4. **(d)** Orbital occupation configuration of Mn^{2+} (d^5) and Co^{2+} (d^7). **(e)** R_{V-V} in CoV_2O_4 and MnV_2O_4 are compared with R_{V-V} in other vanadates from Ref. [20].

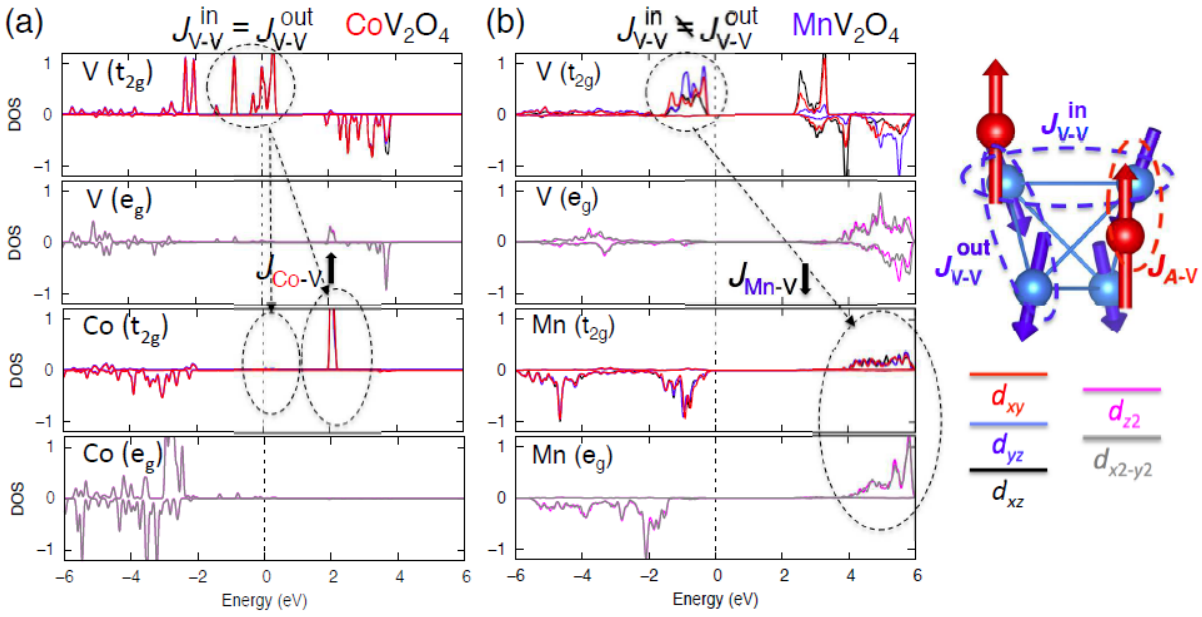

FIG. 3. **Origin of the enhanced magnetic ordering temperature in CoV_2O_4 .** Projected density-of-states of CoV_2O_4 **(a)** compared to MnV_2O_4 **(b)** in unit of eV^{-1}. Dotted arrows denote the energy differences, Δ between V and Co/Mn for possible AFM super-exchange ($J_{A-V} \sim -t^2/\Delta$). t is the hopping parameter between orbitals.

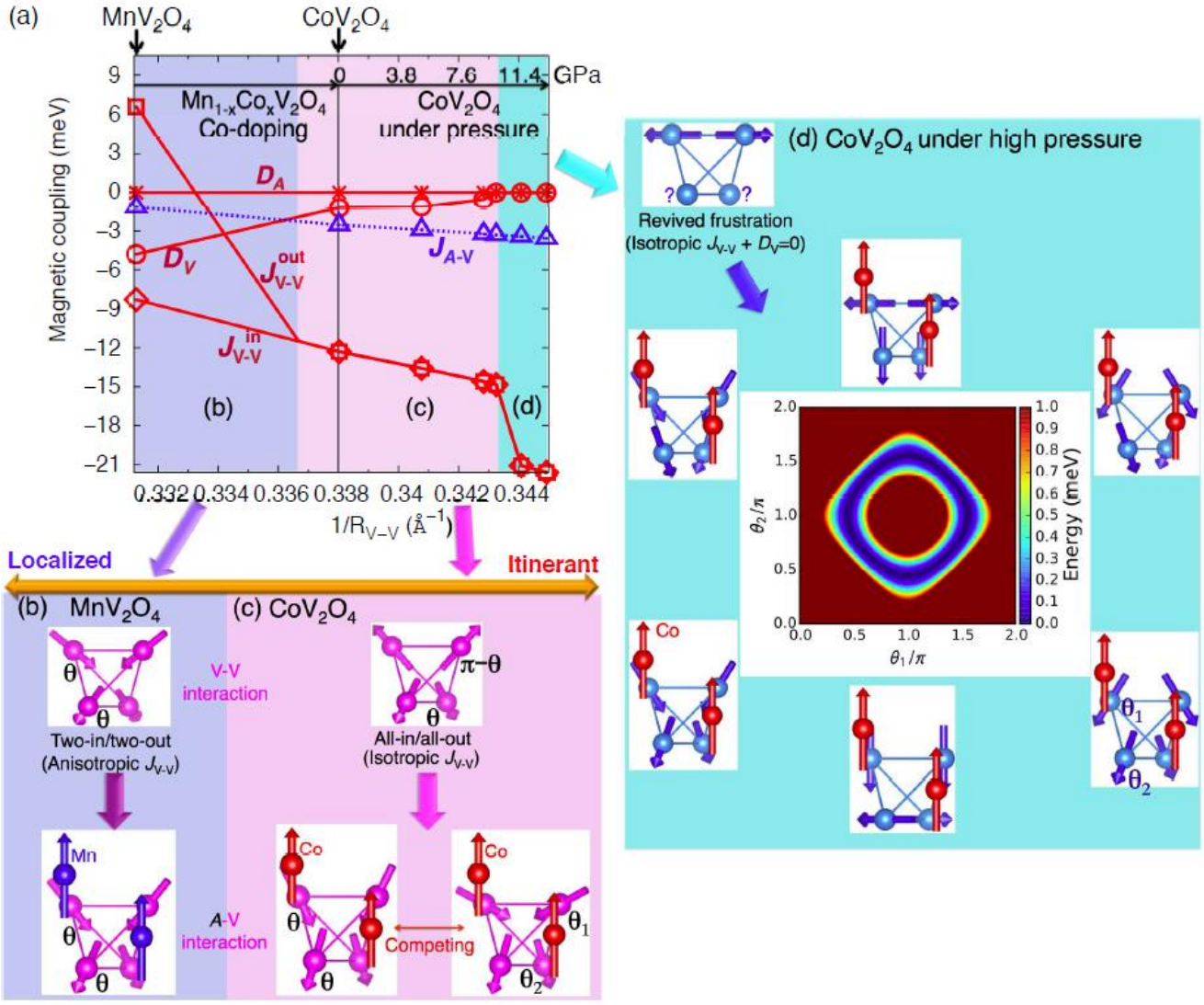

FIG. 4. **Evolution of magnetic couplings and competing ground states driven by Co-doping and pressure** **(a)** Change of all magnetic interactions with Co doping and external pressure (Gpa) calculated by LSDA+U for the ground states at zero temperature. Points represent DFT results and the connecting lines are a guide for eye. $J^{\rm in}_{\rm V-V}$ and $J^{\rm out}_{\rm V-V}$ are expected to be degenerate at x=0.8 (cubic) in $Mn_{1-x}Co_xV_2O_4$ from experiments [16, 19]. Bold (dotted) lines represent the exchange (J) and SIA (D) interactions. **(b)** Origin of TI/TO state in Mn-rich region. **(c)** Competition of the isosymmetric one-angle TI/TO state with the two-angle state that evolves from the AI/AO state. **(d)** Spin glass phase appears with the disappearance of SIA.

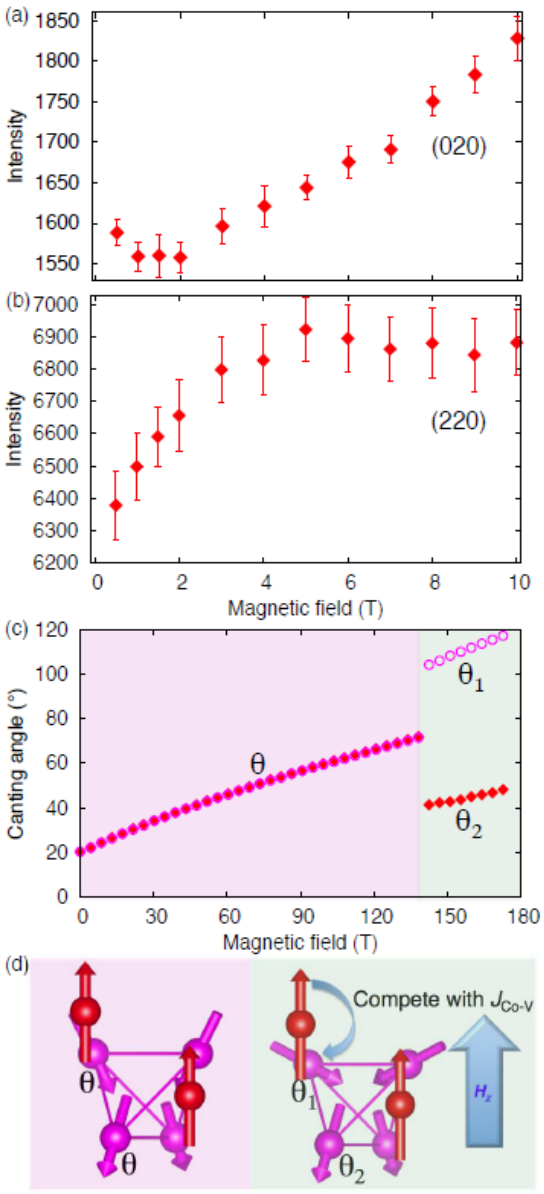

FIG. 5. **Prediction of novel phases driven by magnetic field in $Mn_{0.2}Co_{0.8}V_2O_4$.** **(a)** First-order phase transition from TI/TO to AI/AO-derived state with magnetic field calculated by spin models using DFT parameters. Inset is comparison with neutron scattering measurements (square) up to 10 T. **(b)** One-angle state based on TI/TO (left) and two-angle state based on AI/AO (right). The latter is driven by the weakened $J_{\mathrm{Co-V}}$ in a magnetic field.